Supplementary Material for **ABDULLAH M. ALZAHRANI, SALAHELDIN A. ABDELSALAM, OMAR M. ELMENSHAWY AND ASHRAF M. ABDEL-MONEIM−Ultrastructural Characteristics of Spermiogenesis in *Rhynchophorus ferrugineus* (Coleoptera: Curculionidae).** Florida Entomologist 96(4) (December, 2013) at http://purl.fcla.edu/fcla/entomologist/browse

Corresponding author: Dr. Abdullah M. Alzahrani.
Department of Biological Sciences, Faculty of Science
King Faisal University
Hofouf, Saudi Arabia
E-mail: aalzahra@kfu.edu.sa

ABSTRACT

The red palm weevil (RPW), *Rhynchophorus ferrugineus* Olivier (Coleoptera: Curculionidae), is a pest that is rapidly spreading across the globe. Here, the ultrastructure of *R. ferrugineus* spermatogenesis and sperm are described. The histology of the testis, sperm ultrastructure, and spermiogenesis were investigated using light and transmission electron microscopy. The differentiation of spermatids was observed to occur within spermiogenetic cysts. Inside each cyst, the spermatids were at the same stage of maturation. During early stages, mitochondria aggregated, fused, and elongated beside the growing flagellar axoneme, while the proacrosome transformed into a triple-layered acrosome, with a perforatorium, acrosomal vesicle, and extra-acrosomal layer. The centriolar adjunct was present in early spermatids but was absent from later spermatid stages and sperm. The sperm's tail displayed a typical axoneme with a 9+9+2 microtubule arrangement, 2 mitochondrial derivatives of unequal size, and 2 accessory bodies. A small number of sperm exhibited twin or multiple tails due to membrane fusion. Our results support systematic relationships within the family Curculionidae.

Key Words: axoneme, acrosome, spermatogenesis, microtubules, nebenkern, pterygote spermatozoa, ultrastructure, red palm weevil

RESUMEN

El picudo rojo (RPW), *Rhynchophorus ferrugineus* Olivier (Coleoptera: Curculionidae), es una plaga que se está extendiendo rápidamente en todo el mundo. Se describe la ultraestructura de la

espermatogénesis y los espermatozoides de *R. ferrugineus*. Se investigó la histología de los testículos, ultraestructura de espermatozoides y espermatogénesis, con microscopía óptica y de transmisión electrónica. Se observó que la diferenciación de las espermátidas ocurre dentro de los quistes spermiogenéticos. Dentro de cada quiste, las espermátidas se encontraban en la misma fase de maduración. Durante las primeras etapas, los mitocondrias se agregaron, juntaron, y alargaron al lado del axonema flagelar creciente, mientras que el proacrosoma se transformó en un acrosoma de tres capas, con un perforatorium, vesícula acrosomal y la capa extra-acrosomal. El complemento centriolar estuvo presente en las primeras espermátidas, pero estuvo ausente en las etapas posteriores de los espermátidas y espermatozoides. La cola del espermatozoide pareció como un axonema típico con un 9 + 9 + 2 disposición de microtúbulos, 2 derivados mitocondriales de tamaño desigual y 2 cuerpos auxiliares. Un pequeño número de espermatozoides exhibió colas dobles o múltiples debido a la fusión de la membrana. Nuestros resultados apoyan las relaciones sistemáticas dentro de la familia Curculionidae.

Palabras Clave: axonema, acrosoma, espermatogénesis, microtúbulos, nebenkern, espermatozoides pterygotes, ultraestructura, picudo rojo

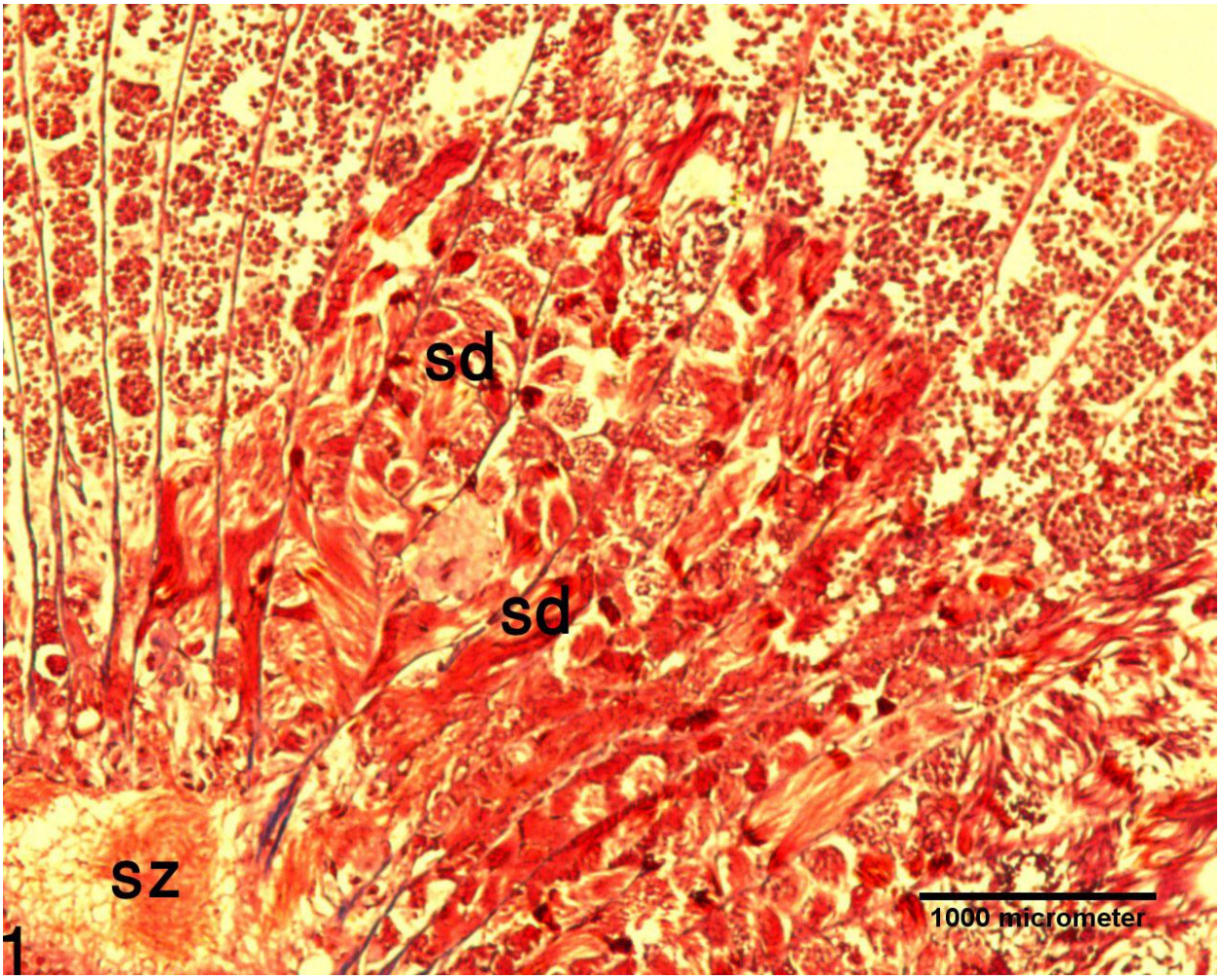

Fig. 1. Photomicrographs. A longitudinal section of the testis of *R. ferrugineus* showing a large number of follicles per testis. Note the bundles of spermatids (sd) inside the mature cysts within the follicles. sz = spermatozoa in the lumen of deferent duct. Hematoxylin and eosin staining.

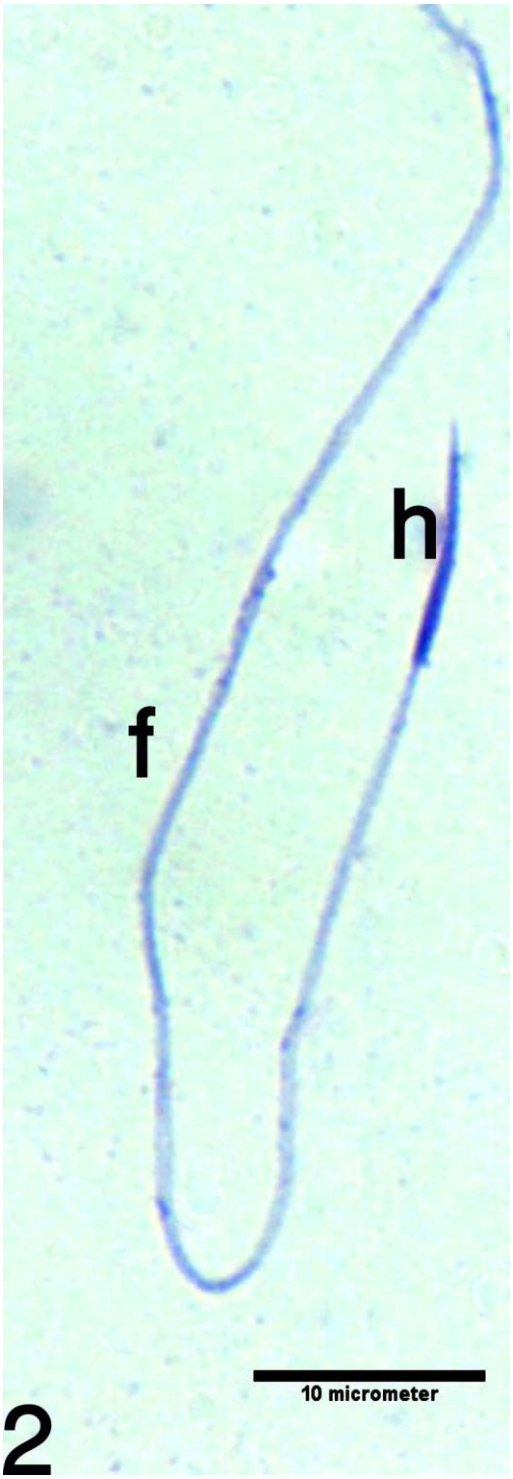

Fig. 2. Photomicrographs. Whole spermatozoon of *R. ferrugineus* with distinct head (h) and flagellum (f). Harris haematoxylin staining.

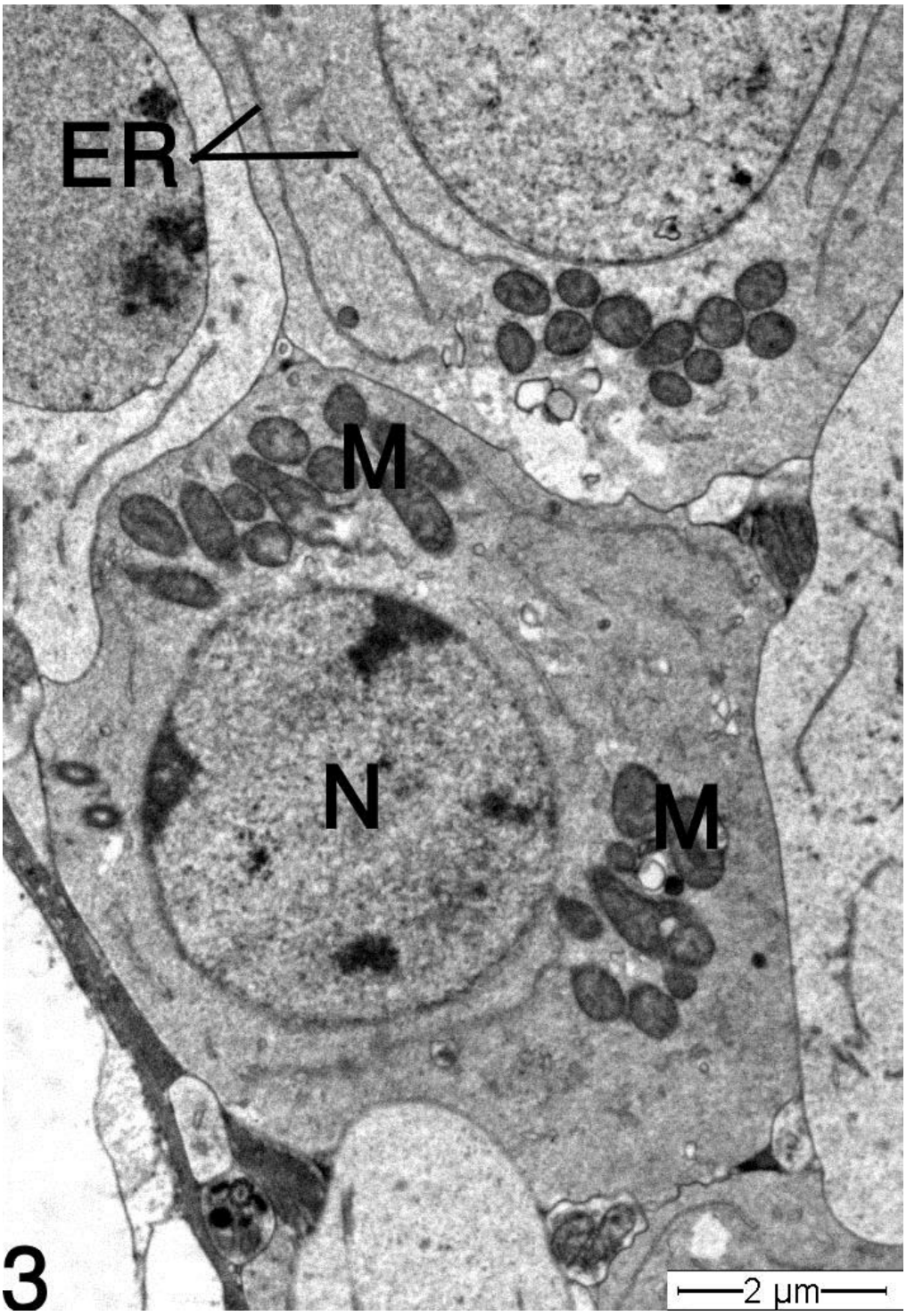

Fig. 3. Transmission electron micrographs of *R. ferrugineus* spermatids. Cross section of early spermatids containing a nucleus (N), a cluster of mitochondrial masses (M), and cisternae of the smooth endoplasmic reticulum (ER).

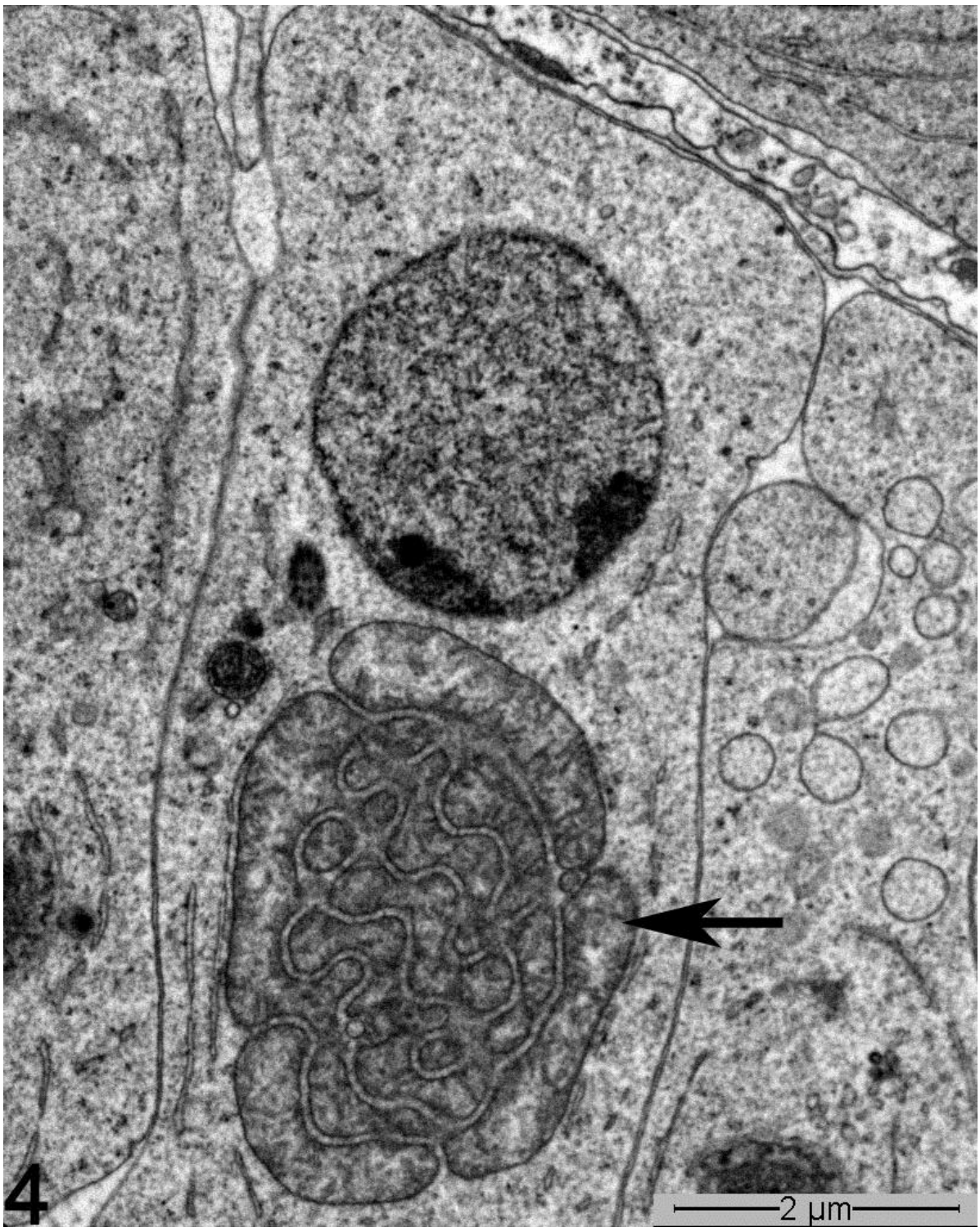

Fig. 4. Transmission electron micrographs of *R. ferrugineus* spermatids. The mitochondrial nebenkern (arrow) is evident in a later stage of spermiogenesis.

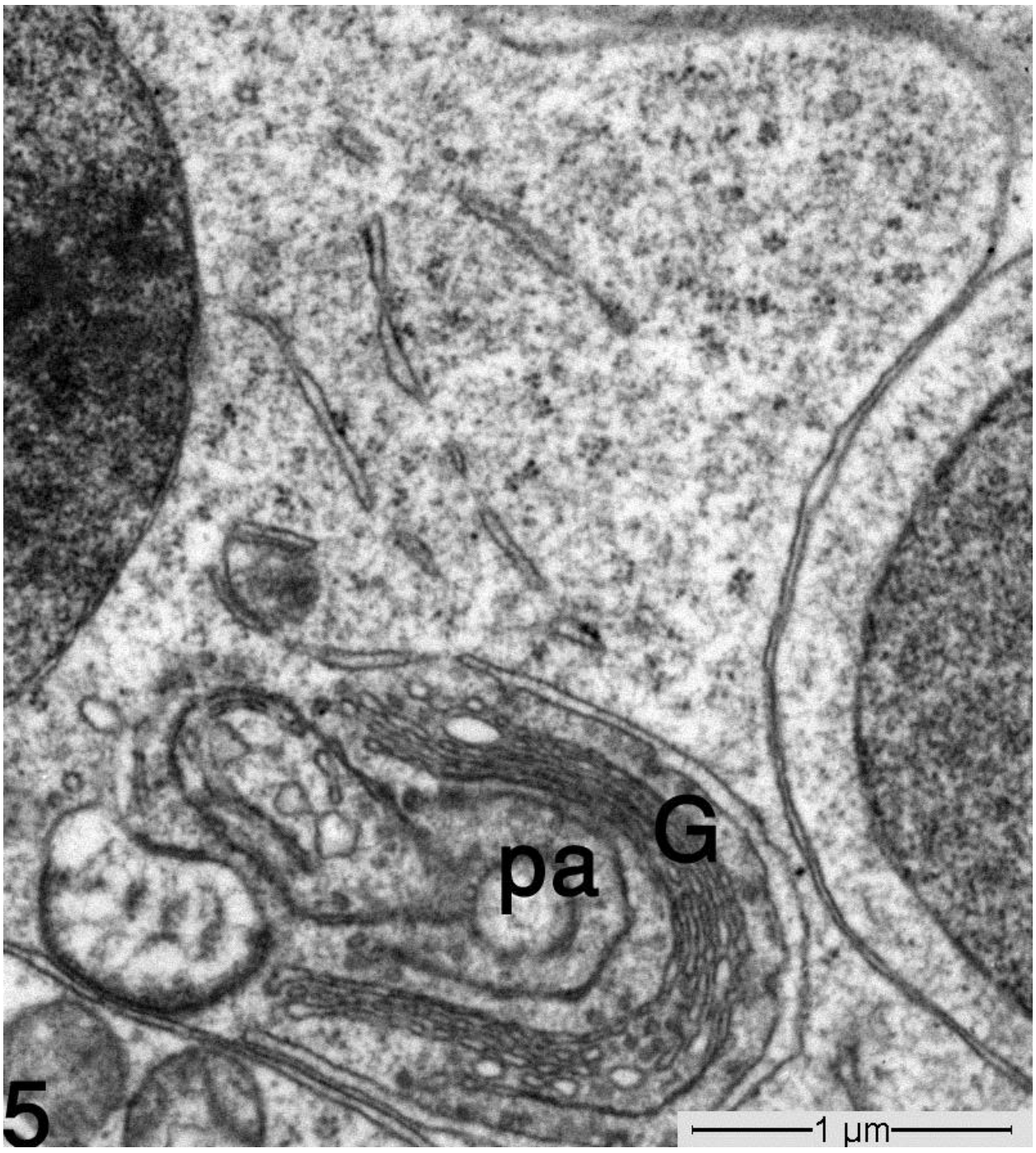

Fig. 5. Transmission electron micrographs of *R. ferrugineus* spermatids. A proacrosomal vesicle (pa) and Golgi membranes (G) are observed near the nucleus.

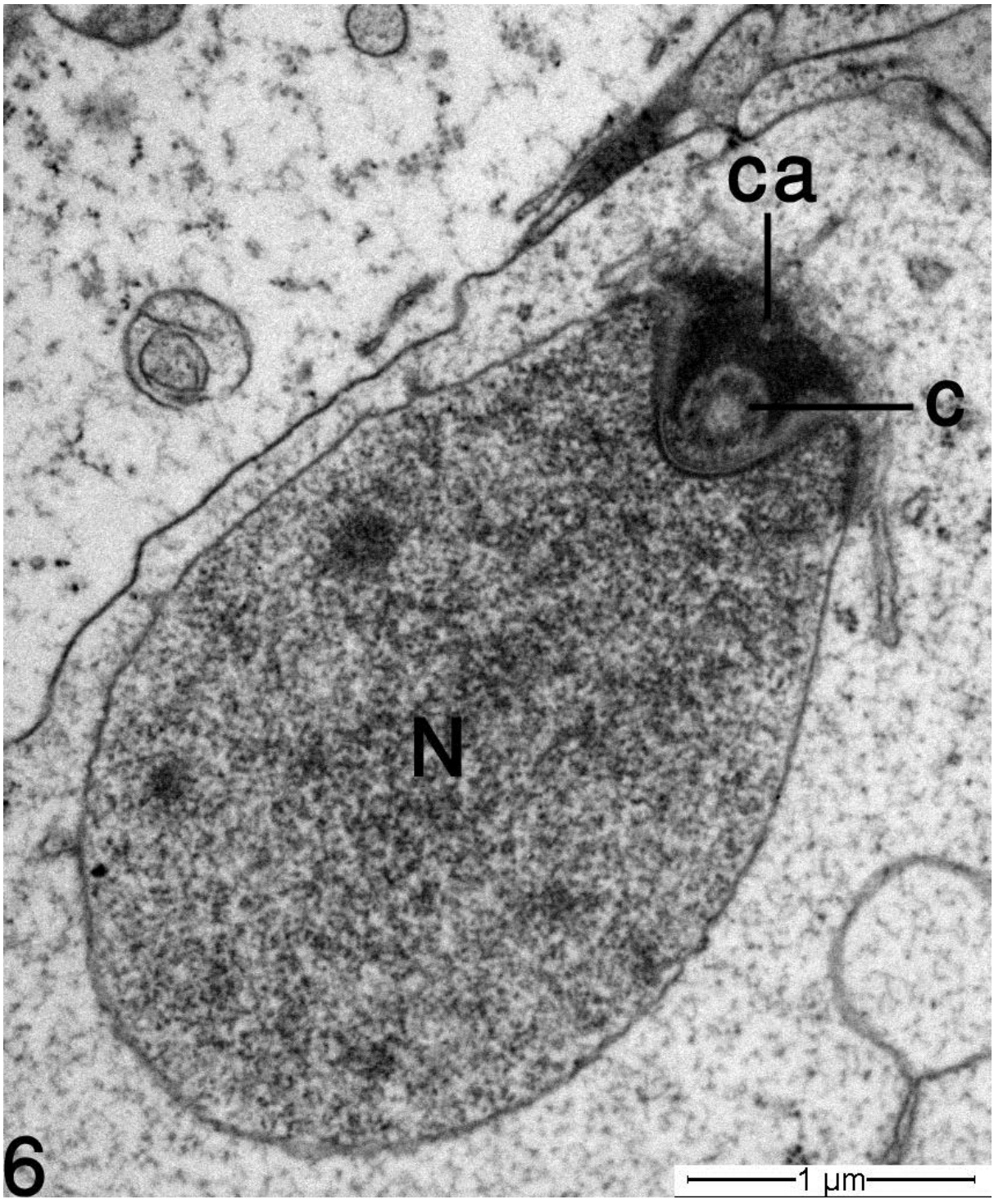

Fig. 6. Transmission electron micrographs of *R. ferrugineus* spermatids. The centriolar region in the initial stage of spermatid differentiation showing the nucleus (N), the centriolar adjunct material (ca), and the centriole (c).

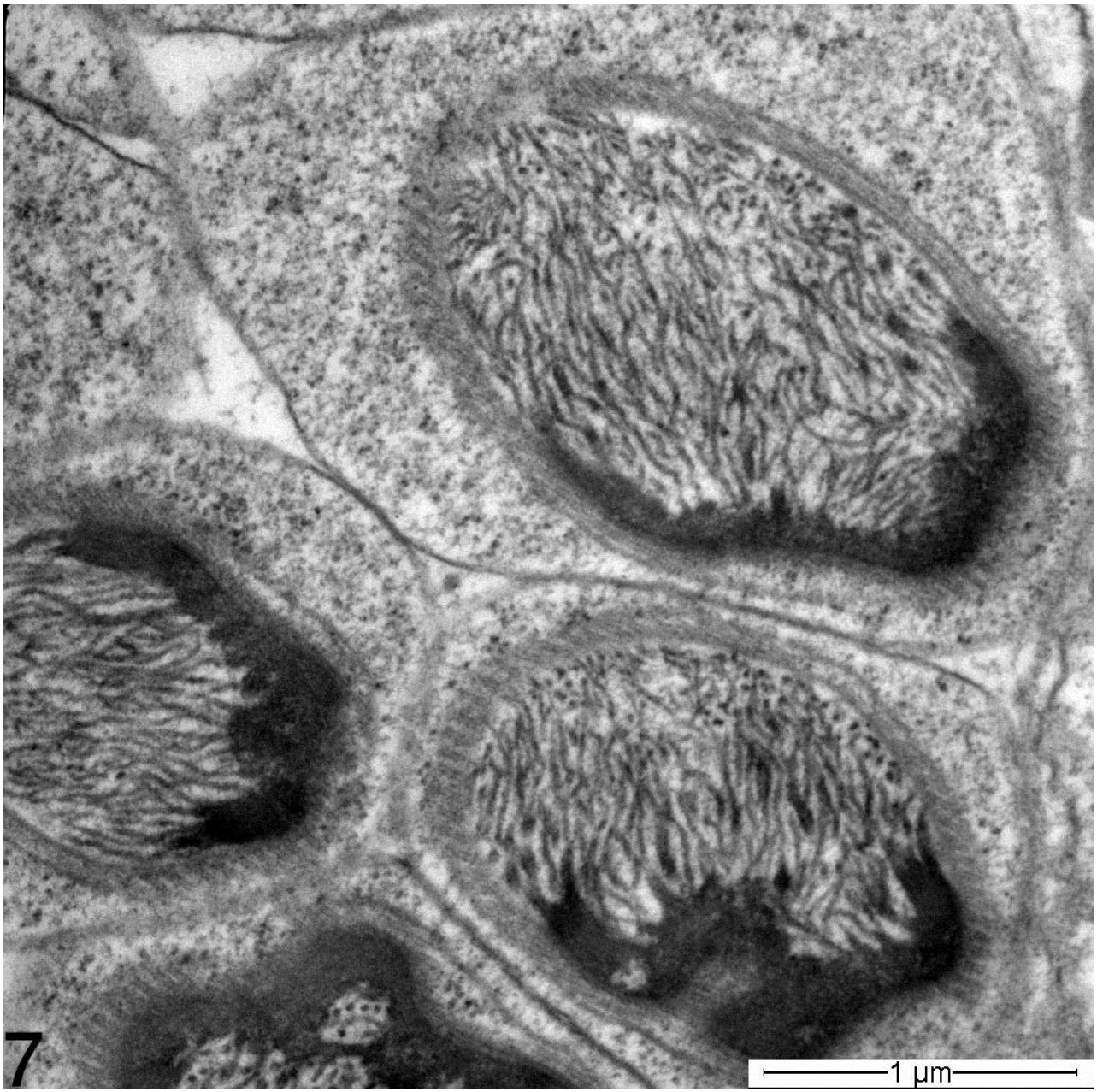

Figs. 7. Transmission electron micrographs of *R. ferrugineus* spermatids. The chromatin shows gradual condensation at the nuclear periphery, converging into the nuclear central region.

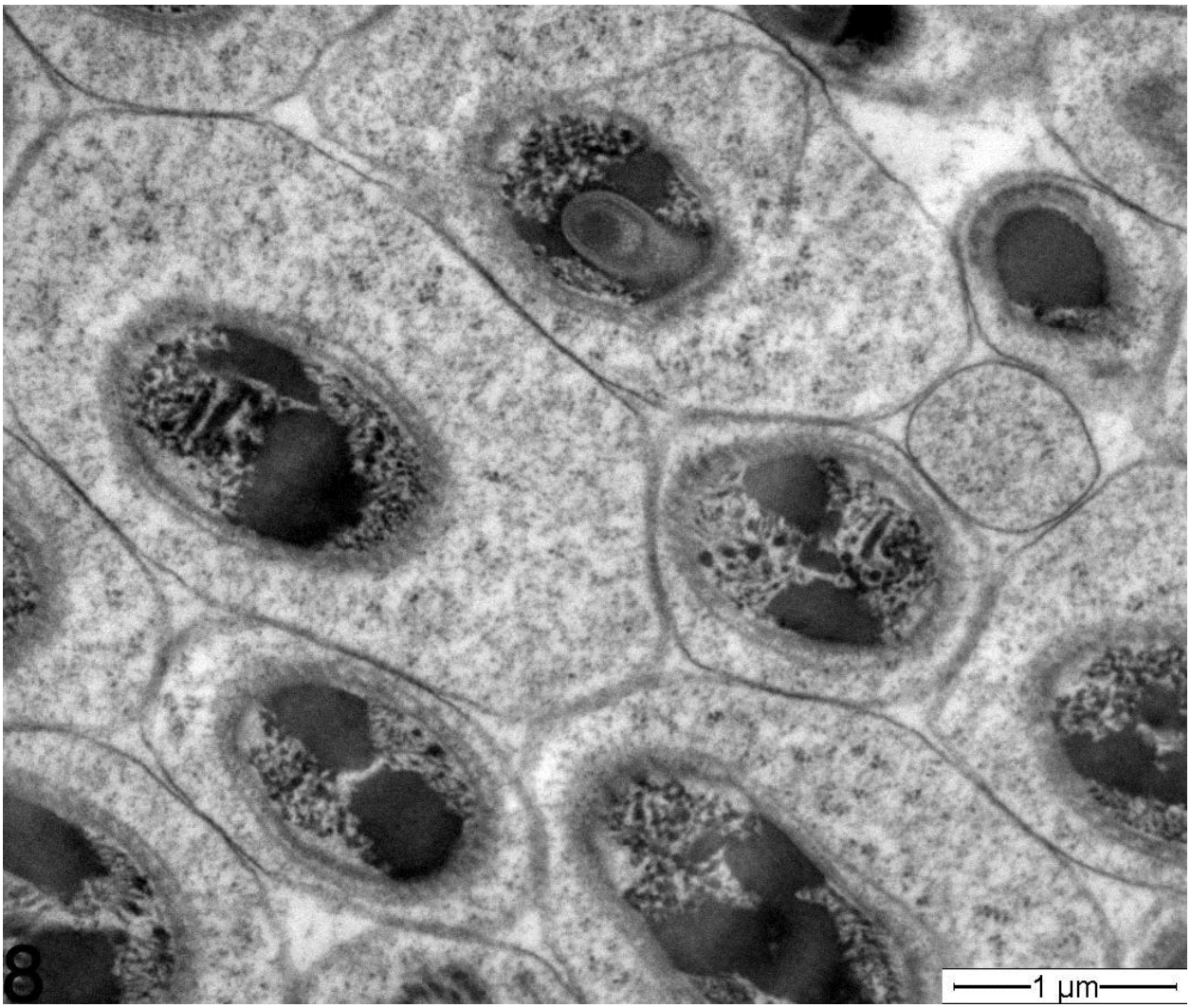

Fig. 8. Transmission electron micrographs of *R. ferrugineus* spermatids. The chromatin shows gradual condensation at the nuclear periphery, converging into the nuclear central region.

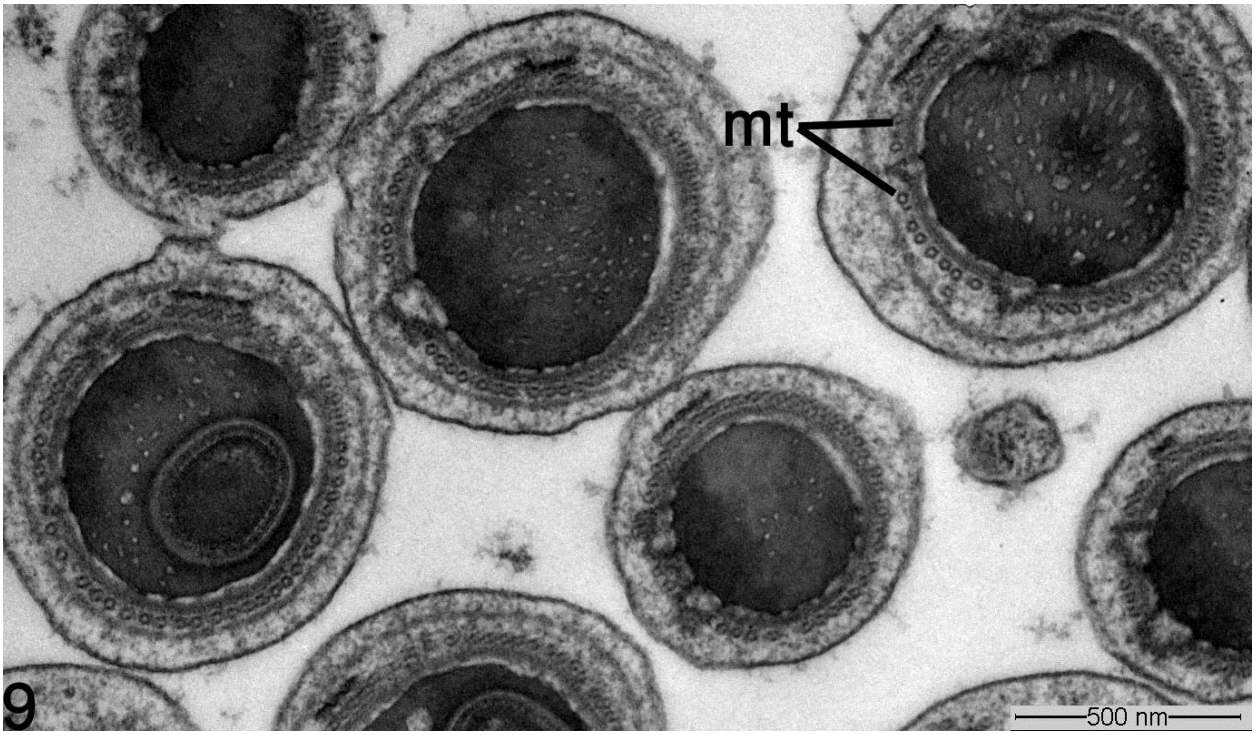

Fig. 9. Transmission electron micrographs of *R. ferrugineus* spermatids. The chromatin shows gradual condensation at the nuclear periphery, converging into the nuclear central region.

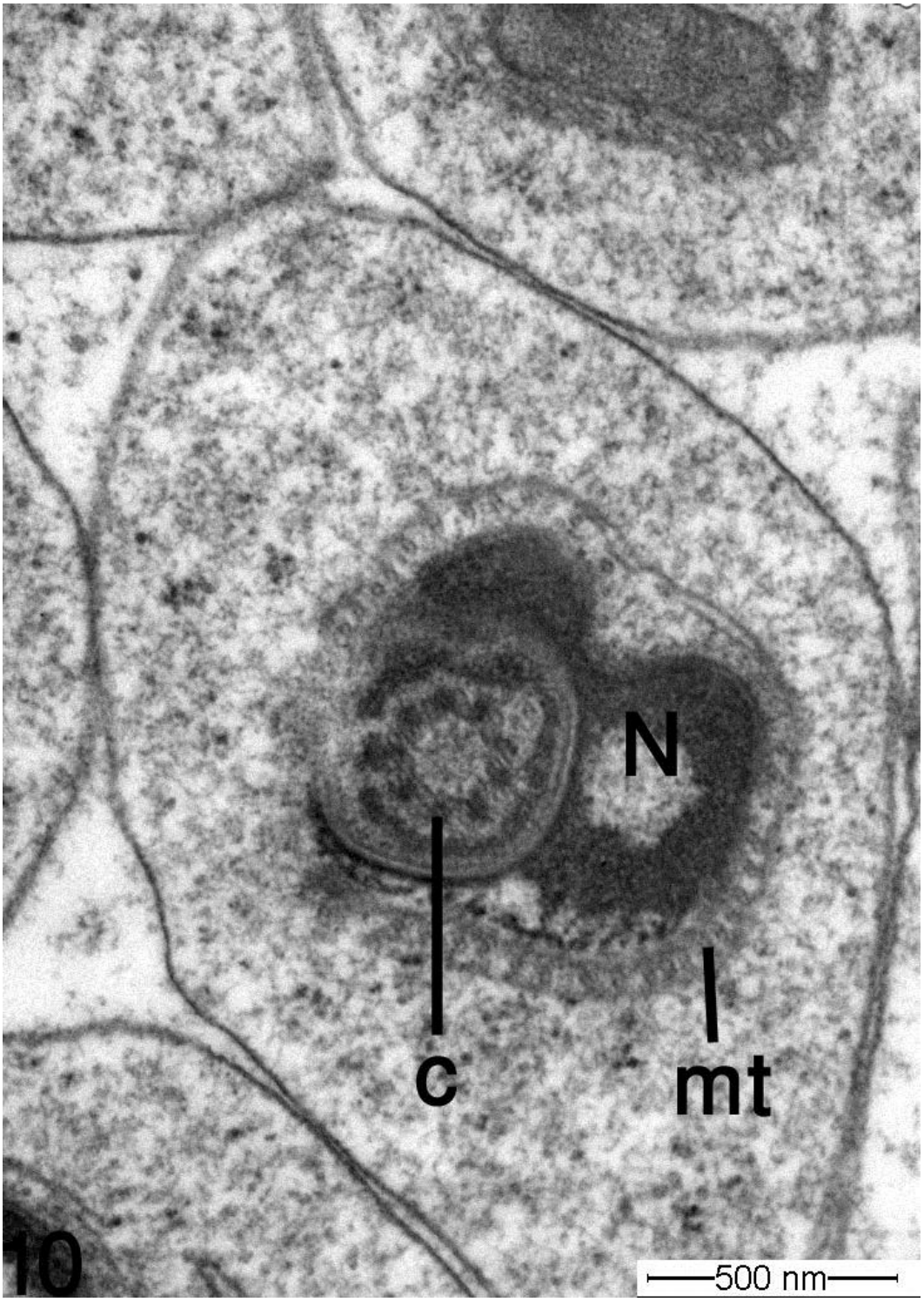

Fig. 10. Transmission electron micrographs of *R. ferrugineus* spermatids. Cross section of the nuclear-flagellum transition in late spermatids. At this level, the centriolar adjunct is absent. N = nucleus, c = centriolar region, mt = microtubules.

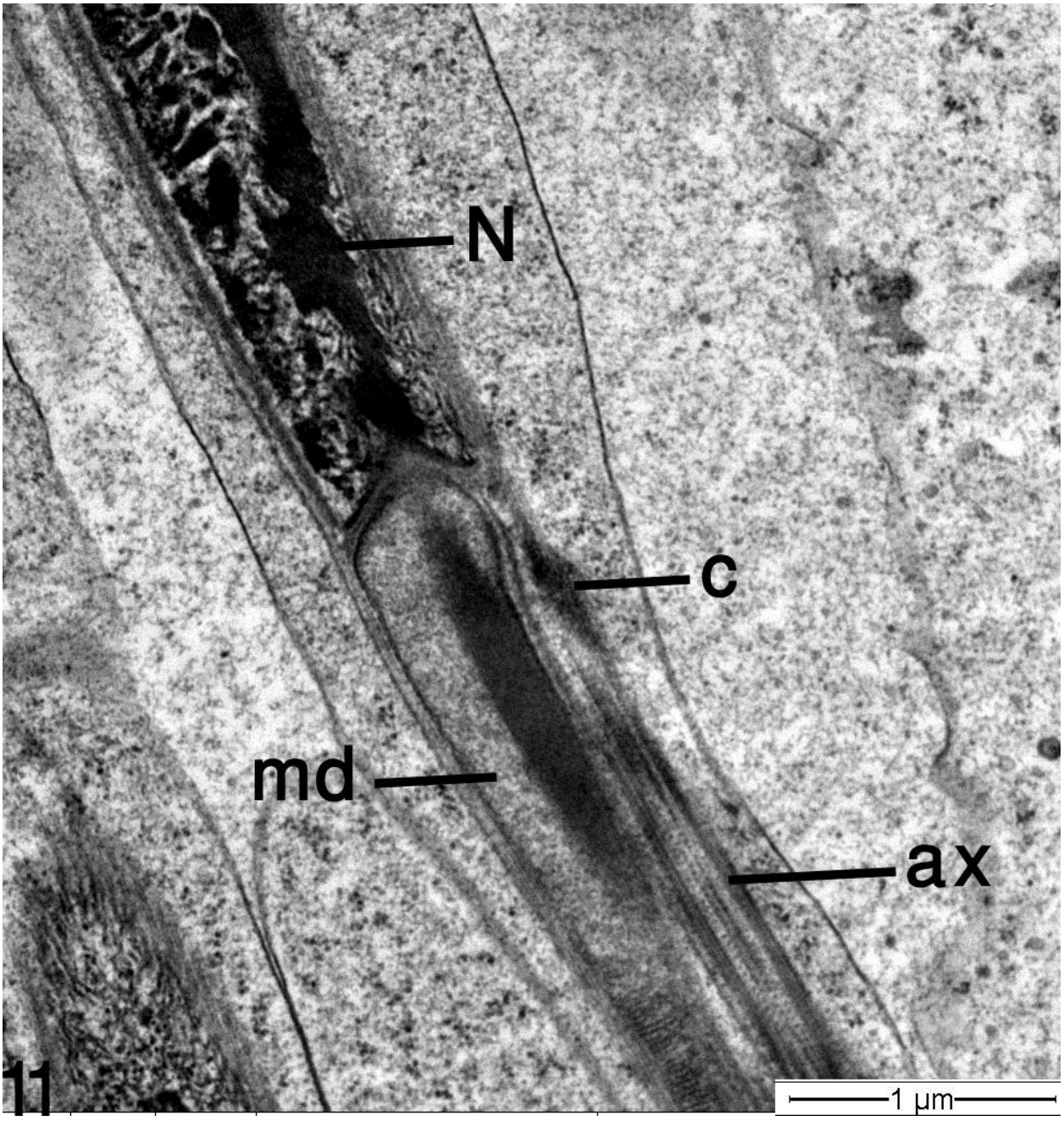

Fig. 11. Transmission electron micrographs of *R. ferrugineus* spermatids. Longitudinal section of late spermatids. The centriole (c) lies posterior to the nucleus, and the axoneme (ax) emerges from it. The mitochondrial derivative (md) is later positioned at the axoneme.

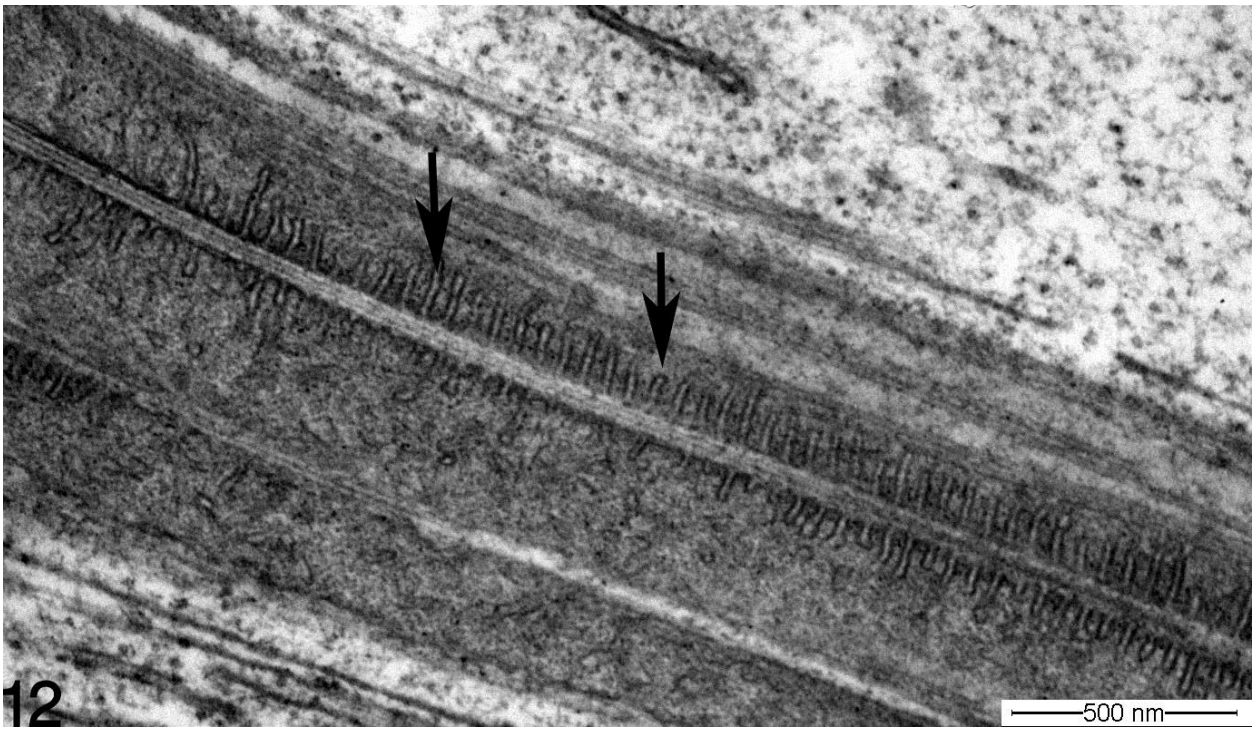

Fig. 12. Transmission electron micrographs of *R. ferrugineus* spermatids. Longitudinal section of mitochondrial derivatives, showing a region of cristae (arrows).

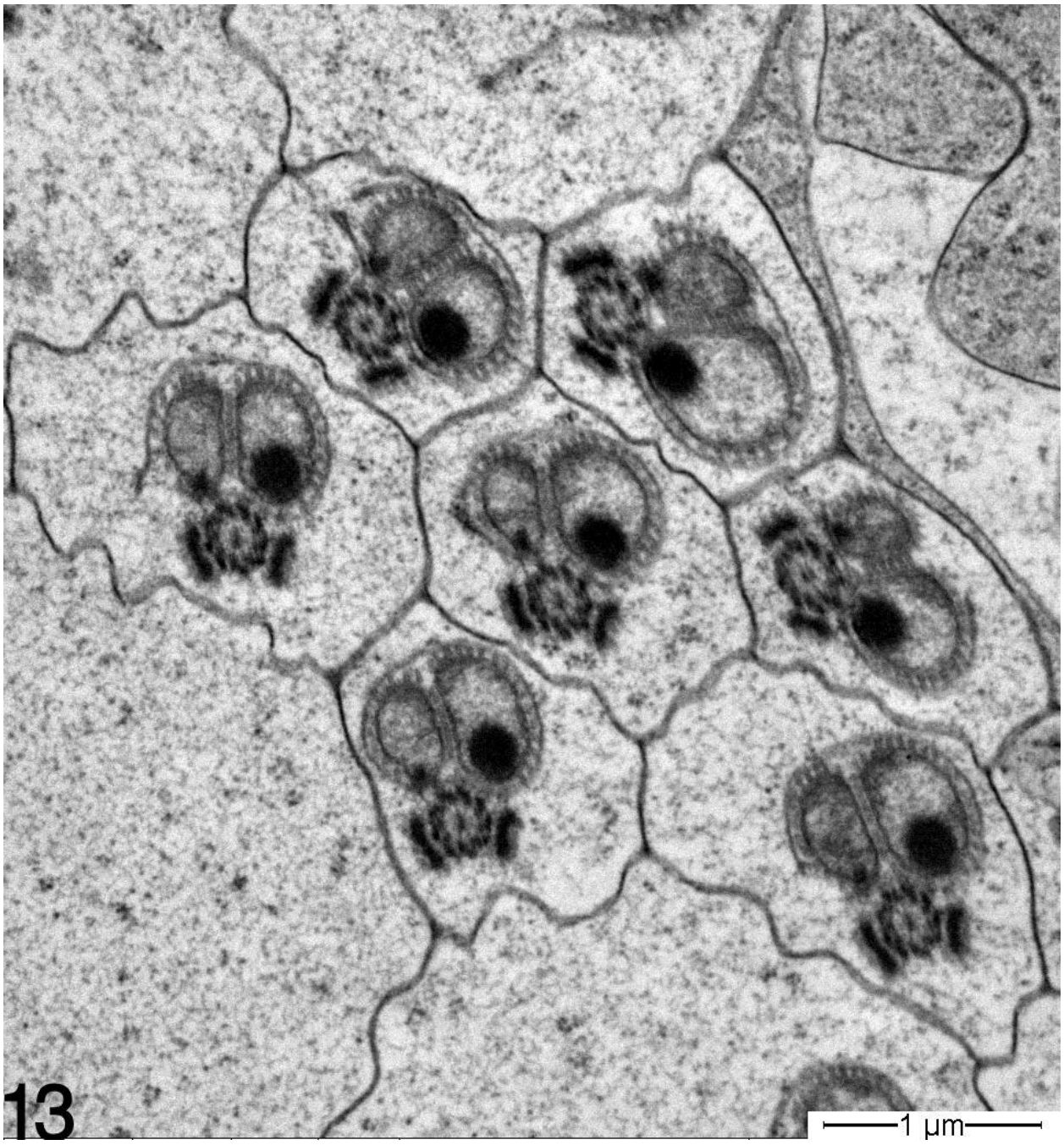

Fig. 13. Transmission electron micrographs of *R. ferrugineus* spermatids. Cross section through the flagellar region of mono-flagellate spermatids.

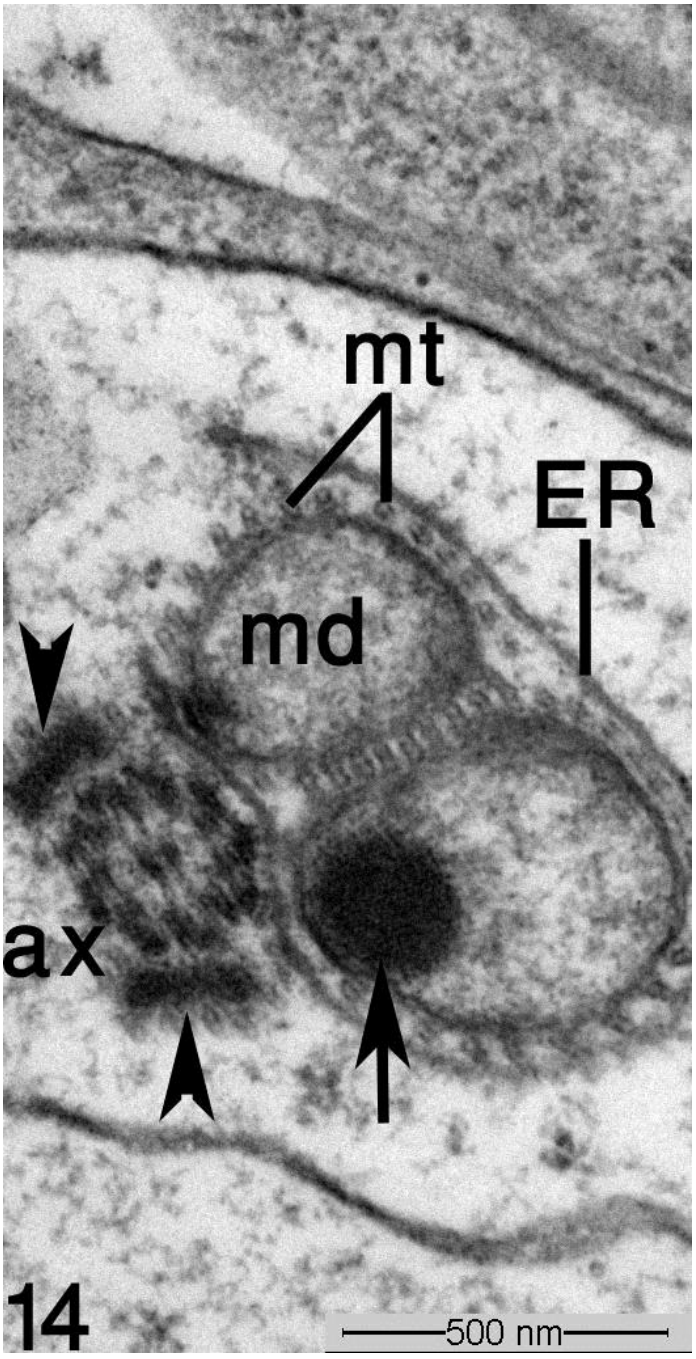

Fig. 14. Transmission electron micrographs of *R. ferrugineus* spermatids. Higher magnification of the spermatid flagellum. The axoneme (ax) consists of a complex of 9+9+2 microtubules. Beneath the axoneme, 2 unequal mitochondrial derivatives (md) are evident, with advanced crystallization (arrow) being observed in the larger one. Lateral to the axoneme, 2 characteristic dense arches (arrowheads) are visible. Note also that microtubules (mt) mostly surround the axoneme and the mitochondrial derivatives. ER = agranular ER.

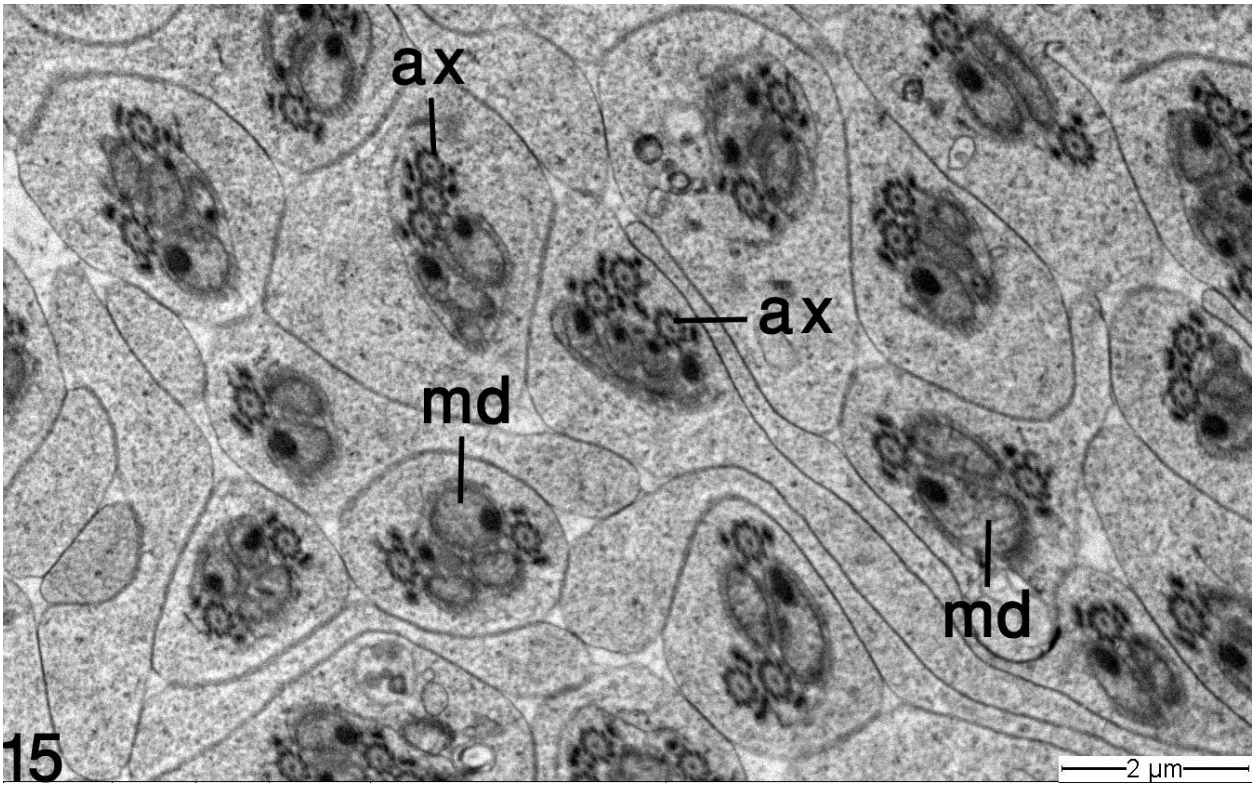

Fig. 15. Transmission electron micrographs of *R. ferrugineus* spermatids. Group of bi- and tri-flagellate spermatids in an advanced state. Two to 3 mitochondrial derivatives (md) are visible. Arrows point to the tail axonemes.

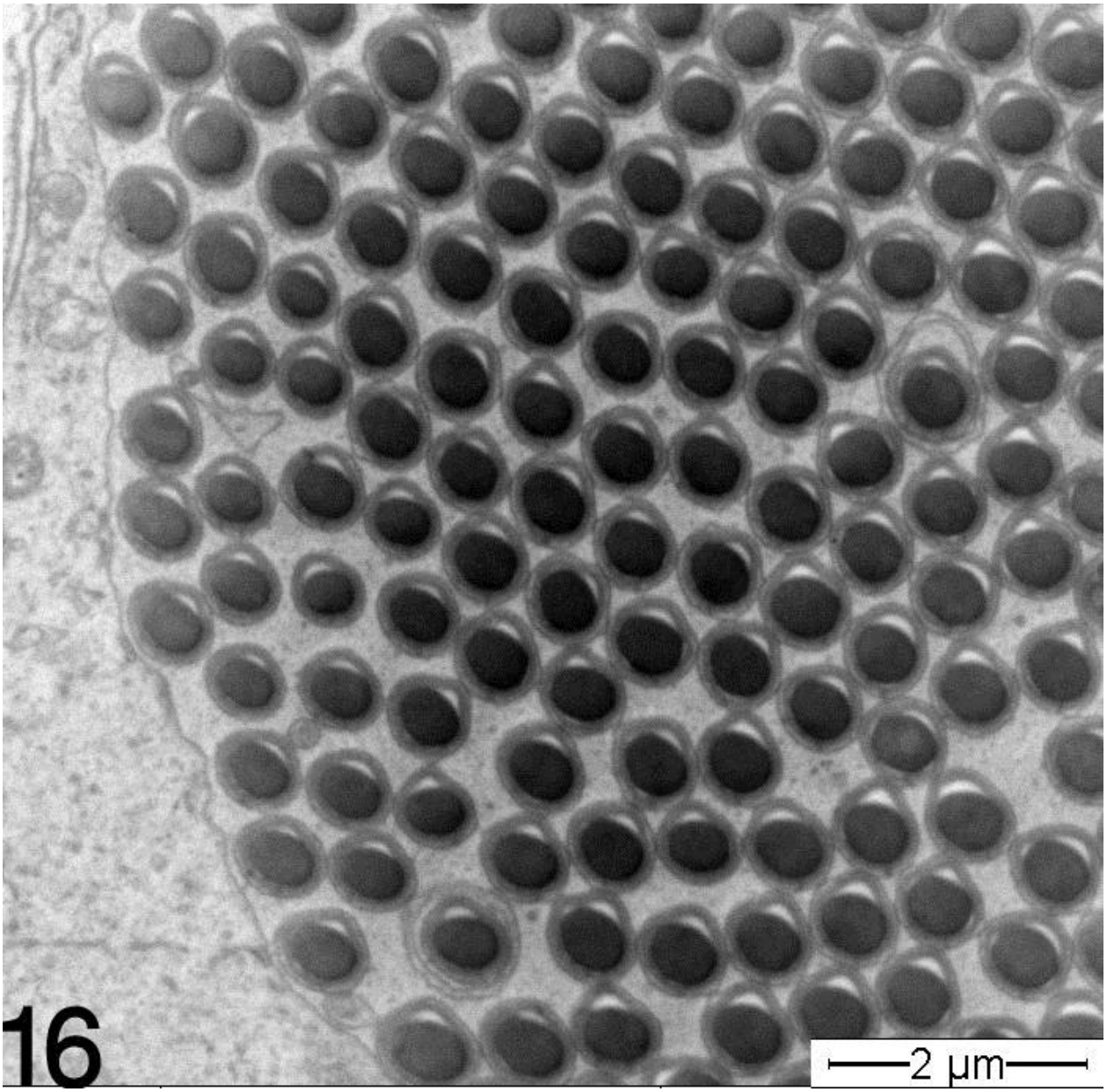

Fig. 16. Transmission micrographs of *R. ferrugineus* spermatozoa. Cyst containing a cross section of the spermatozoa head region.

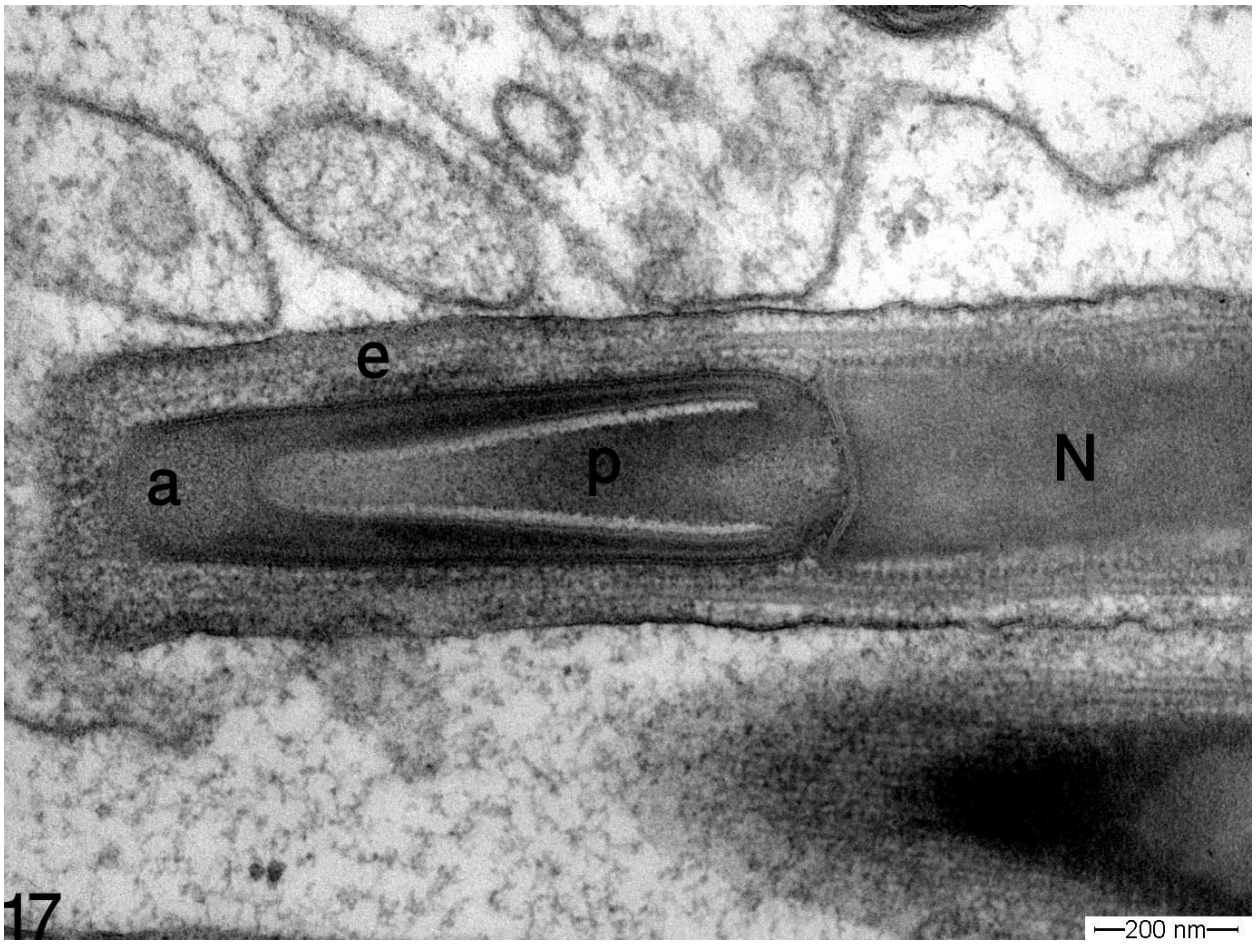

Fig. 17. Transmission micrographs of *R. ferrugineus* spermatozoa. Longitudinal section of a sperm head showing the perforatorium (p), acrosomal vesicle (a), and extra-acrosomal tissue (e). N = nucleus.

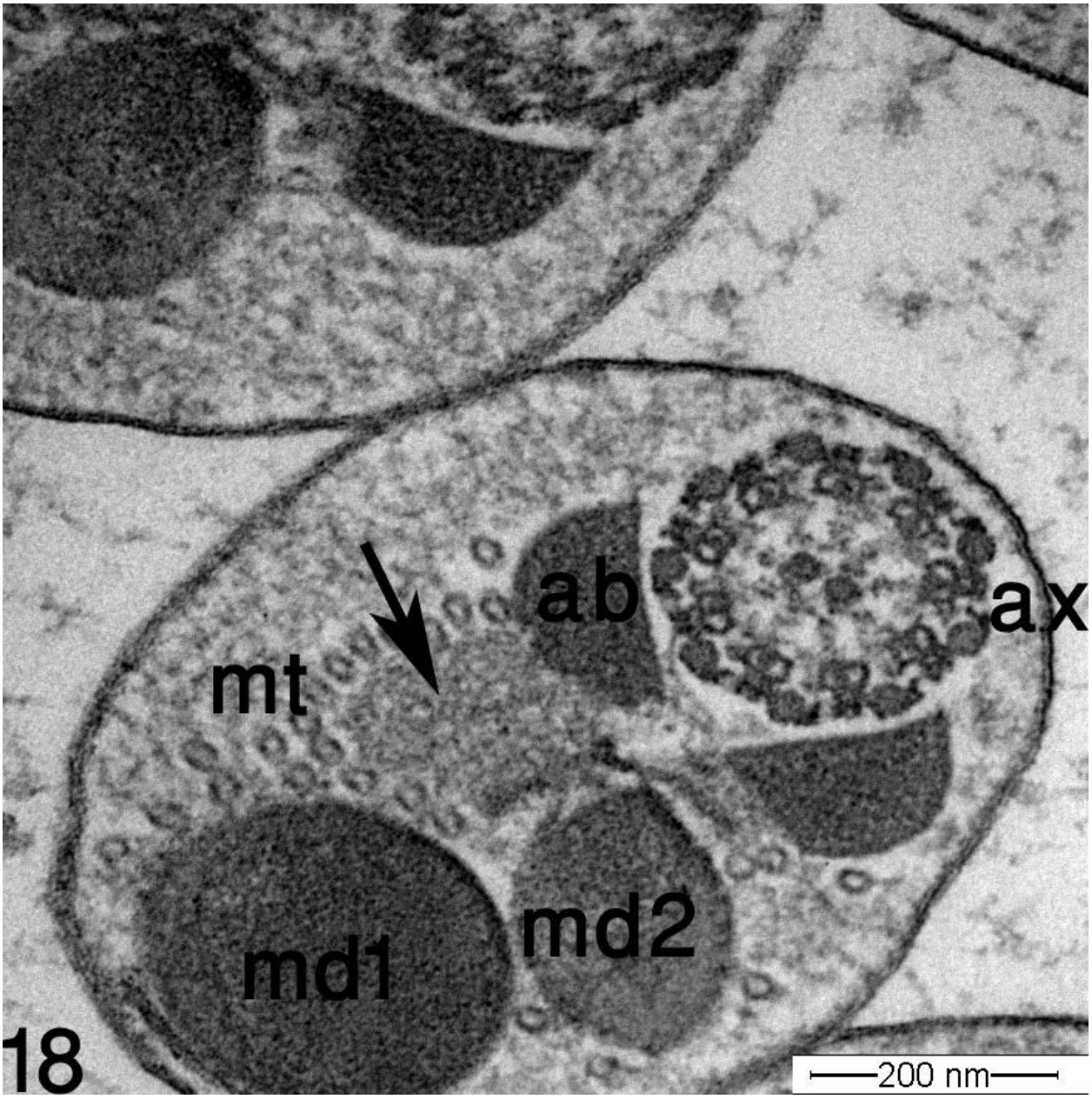

Fig. 18. Transmission micrographs of *R. ferrugineus* spermatozoa. Cross section of a sperm flagellum showing the 9+9+2 axoneme (ax), accessory bodies (ab), mitochondrial derivatives (large md1 and small md2), and the puff-like corpuscle (arrow). Mt = microtubules.

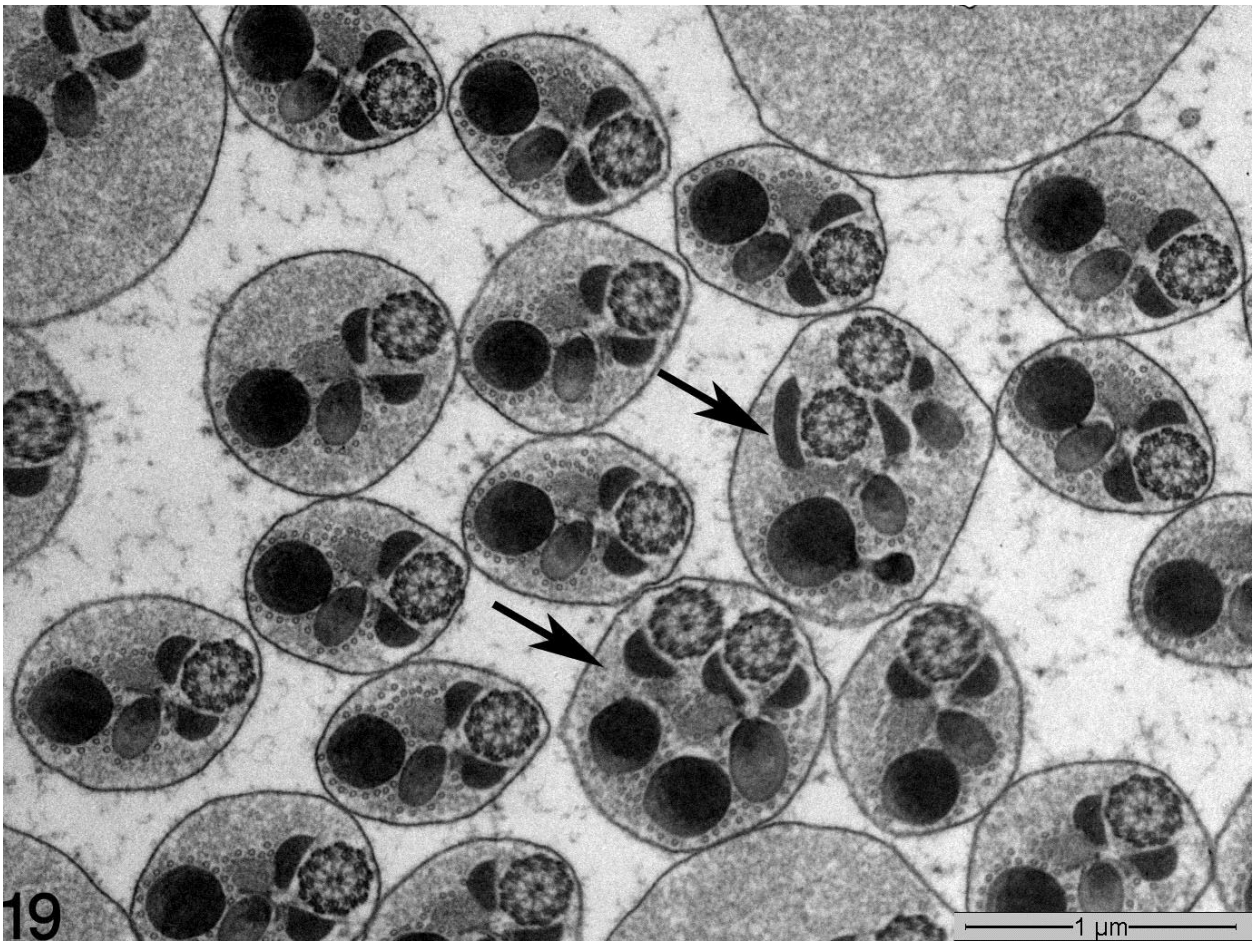

Fig. 19. Transmission micrographs of *R. ferrugineus* spermatozoa. Arrows indicate bi-flagellate sperm with 2 axonemes.